Hybrid phosphorescence and fluorescence native spectroscopy for breast cancer detection

Alexandra Alimova
A. Katz
Vidyasagar Sriramoju
Yuri Budansky
Alexei A. Bykov
Roman Zeylikovich
R. R. Alfano
The City College of New York
Department of Physics
Institute for Ultrafast Spectroscopy and Lasers
New York, New York 10031
E-mail: alfano@sci.ccny.cuny.edu

Abstract. Fluorescence and phosphorescence measurements are performed on normal and malignant *ex vivo* human breast tissues using UV LED and xenon lamp excitation. Tryptophan (trp) phosphorescence intensity is higher in both normal glandular and adipose tissue when compared to malignant tissue. An algorithm based on the ratio of trp fluorescence intensity at 345 nm to phosphorescence intensity at 500 nm is successfully used to separate normal from malignant tissue types. Normal specimens consistently exhibited a low I_{345}/I_{500} ratio (<10), while for malignant specimens, the I_{345}/I_{500} ratio is consistently high (>15). The ratio analysis correlates well with histopathology. Intensity ratio maps with a spatial resolution of 0.5 mm are generated in which local regions of malignancy could be identified. © *2007 Society of Photo-Optical Instrumentation Engineers.* [DOI: 10.1117/1.2437139]

1 Introduction

Optical biopsy—the use of native tissue fluorescence—for detection of cancer has been an area of investigation for over two decades.[1–3] The bases behind the operation of optical biopsy is that the onset of carcinogenesis results in structural changes (thickening of the mucosa layer, increased vascularity) and molecular changes (increased nucleic acids, alterations in protein structure, increased cell metabolism) that modify the spectroscopic properties of tissue and, thereby, create unique optical signatures that can be used to detect malignant and premalignant tissues. In the UV and blue spectral regions, the major native tissue fluorophores are tryptophan (trp), collagen, elastin, reduced nicotinamide adenine dinucleotide (NADH), and flavins. Optical biopsy has been demonstrated to be an accurate, real-time tool for distinguishing normal tissues from malignant and premalignant tissues. Prior investigations have demonstrated that there are several ratio-based algorithms that can distinguish malignant tissue from normal with high sensitivity and specificity.[3–5] The wavelength combinations used in those ratios isolated the contributions from different pairs of tissue fluorophores, one of which was trp. The ratio of 340- to 440-nm emission (with 300-nm excitation) has been shown to be a useful ratio to identify malignant tissues from many different organ sites.[4,6] However, when the I_{340}/I_{440} ratio was applied to *ex vivo* human breast tissue, the presence of adipose tissue required that multiple wavelength ratio pairs be evaluated to successfully distinguish adipose tissue from malignant tissue by

fluorescence.[7] Identification of additional spectroscopic fingerprints to distinguish adipose and normal glandular tissues from malignant breast tissue can significantly enhance optical biopsy of breast tissues and improve the efficacy of either fine needle aspiration or micro-endoscopic ductal examination.

For excitation between 250 and 300 nm, trp is the predominant native fluorophore in tissues. The trp fluorescence and phosphorescence properties, such as Stokes shift and quantum efficiency, are strongly dependent on the local environment and protein structure.[8] Therefore, trp emission is expected to differ in different types of tissue environments. The trp Stokes shift is highly dependent on solvent polarity, with a more polar solvent producing a greater Stokes shift, i.e., red-shifted fluorescence.[9–11] In proteins with multiple trp residues, the emission spectrum is the sum of each residue's individual spectrum.

Trp phosphoresces in the range from 400 to 500 nm. At room temperature, phosphorescence from trp solution is difficult to observe due to quenching by dissolved oxygen and other quenchers.[12] In complex proteins, aromatic amino acid residues can be buried within the protein structure, and thus have limited exposure to potential quenching molecules. In such proteins, trp phosphorescence may be observed at room temperature.[12–16] In the absence of quenching, the phosphorescence lifetime of trp is 5.5 s at 77 K, and between 0.1 to 0.8 s at room temperature.[12,17] Proximity to potential quenchers and rigidity of the protein structure can also affect the trp phosphorescence with lifetime changes of 3 to 4 orders of magnitude.[17,18] Protein folding hinders the quenching of phosphorescence for internal trp residues.[12] In proteins, trp phosphorescence is enhanced[19] at both high and low pH com-

Address all correspondence to: R. R. Alfano, The City College of New York, Institute for Ultrafast Spectroscopy and Lasers, 160 Convent Ave., New York, NY 10031. Tel: 212-650-5531; Fax: 212-650-5530; E-mail: alfano@sci.ccny.cuny.edu

pared to neutral pH. Phosphorescence lifetime of trp residues is sensitive to protein conformational changes.[20] These properties makes room temperature trp phosphorescence an effective tool to investigate protein structure.[12,21]

Breast cancer causes changes in local environment and proteins which may affect trp phosphorescence. Breast cancer changes the pH (from neutral or slightly alkaline in normal cells to slightly acidic in cancer cells) as well as changes in the respiratory mechanisms of cells.[22] Cancer cells consume less oxygen than normal cells, becoming anaerobic and utilizing glucose to produce lactic acid, which decreases pH. This decrease in pH and changes in the respiration mechanism can affect protein structure with subsequent changes in phosphorescence. Thus phosphorescence may be an additional spectroscopic signature to distinguish malignant tissue from benign.[23] Although phosphorescence is much weaker than fluorescence, the longer lifetime of phosphorescence (milliseconds to seconds) as compared to fluorescence ($\sim$3 ns) enables the two signals to be separated by using a pulsed excitation and time-gated photodetection.

In this paper, for the first time, the phosphorescence and combined phosphorescence and fluorescence spectra from *ex vivo* human breast tissues were measured and differences in the ratio of trp phosphorescence to fluorescence intensities were observed between malignant tissue and normal glandular and adipose tissues. Ratio maps were generated from the tissue spectra that designated regions of tumor from normal glandular and adipose tissue. This paper proposes a new optical approach to detect cancer extending the fluorescence approach.[1–3]

This paper also reports the first use of AlGaN alloy UV LEDs to excite native tissue fluorophores. The use of UV LEDs instead of lamps can significantly advance the development of compact optical biopsy instrumentation. The narrower bandwidth of LEDs compared to xenon or mercury lamps can reduce stray light leakage. LEDs are more efficient at coupling light into optical fibers than lamps. Their small size and lower current requirements can reduce the size of instrumentation for use in miniature photonic devices.[24]

2 Materials and Methods

2.1 Experimental Setup

Two experimental setups were used to acquire the spectra from trp powder and tissues. One setup used a CD-Scan (Mediscience Technology Corp, Cherry Hill, New Jersey). The CD-Scan is a modified LS50B (Perkin Elmer, Shelton, Connecticut) fluorescence spectrophotometer. The CD-Scan uses a pulsed xenon excitation lamp (τ_p=10 μs) and gated photomultiplier tube (PMT) detectors. The delay between the lamp pulse and the detector gate is computer selectable, enabling collection of either fluorescence (zero delay between lamp pulse and detector gate) or phosphorescence (delays greater than the lamp pulse width). The illumination area of the CD-Scan is a function of the excitation monochromator slit width. For the phosphorescence measurements, the excitation monochrometer resolution was set to 10 nm, giving an excitation area of approximately 5×10 mm. The scan rate was 120 nm/min. The photodetector gate delay can be varied in 1.0-ms steps.
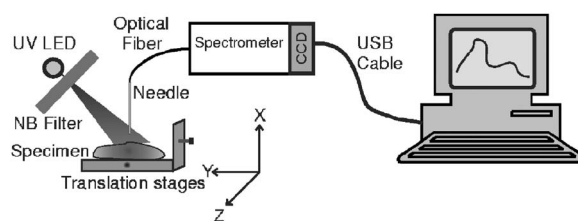

Fig. 1 Experimental setup for mapping tissue fluorescence and phosphorescence.

The second experimental setup shown in Fig. 1 was used to generate ratio maps from the breast tissue specimens. The excitation source was an AlGaN alloy UV LED with emission centered at 300 nm with 400 μW of average power. A narrow-band (NB) interference filter (10 nm FWHM) was used to block the longer wavelength fluorescence emitted by the LED. The emission was collected through a 200-μm optical fiber inserted inside a metal jacket. The collection region was approximately 0.5 mm in diameter. The metal jacket is similar in size to a stereotactic needle such as the type used for fine needle aspiration (FNA) procedures on human breast and the collection fiber can easily be integrated into an FNA system. The digital output of the CCD is connected to a PC via a USB (universal serial bus) connection. The integration time of the CCD is computer controllable and was set to 2 s so that both fluorescence and phosphorescence were detected simultaneously. The spectrograph exhibited relatively more efficiency in the visible region than in the UV, compared to the CD-Scan. Thus, after normalizing the spectra to the trp fluorescence peak ($\sim$350 nm), the trp phosphorescence normalized "counts" were higher with the spectrograph setup than with the CD-Scan. Specimens were mounted on a two-axis translation stage, enabling spectra to be acquired at different locations on the samples.

2.2 Tissue Specimens

Fresh surgical specimens of cancerous and normal breast tissues were acquired under Institutional Review Board approval, from a tissue bank within 24 h of surgery. The normal specimens, acquired from subjects undergoing breast reduction surgery, had clearly defined regions of normal glandular and adipose tissue. The malignant specimens were acquired from patients undergoing lumpectomies. These specimens were from the margins of the tumor and were a mix of malignant and normal tissues. Specimens were stored at 4 °C and were not subjected to any additional processing prior to measuring the spectra. Specimens were cut into pieces ranging from $\sim$0.5 to $\sim$1 cm^2 and placed in a 1-$\times$1-cm quartz cuvette, prior to mounting on the translation stage. Using the spectrograph setup, the spectra were acquired in a grid pattern with a 0.5- to 1.0-mm spacing so as to cover most of the specimen. Each spectrum was integrated for 2 s. Intensity ratio maps were generated from the individual spectra. Five cancerous and six normal breast tissue specimens were scanned for a total of $\sim$3000 locations on the tissue specimens. After completion of a sequence of scans with the spectrograph apparatus, the fluorescence and phosphorescence were measured with the CD-Scan. In fluorescence mode, the photodetector gate was synchronized with the excitation lamp
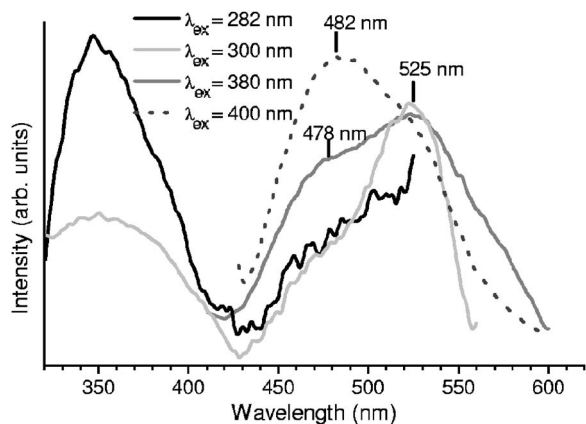
Fig. 2 Phosphorescence spectra of D-L tryptophan powder for different excitation wavelengths. Spectra are integrated from 0.5- to 7.5-ms delay with respect to excitation lamp pulse.

pulse (zero time delay). The much higher efficiency of fluorescence compared to phosphorescence meant that the signal was dominated by the fluorescence. In phosphorescence mode, the photodetector gate delay was varied from 0.5 to 6.5 ms with respect to the xenon lamp pulse.

3 Results and Discussion

3.1 Trp Powder

Figure 2 shows the room-temperature phosphorescence spectra of D-L trp powder excited at 282, 300, 380, and 400 nm and acquired with the CD-Scan. Each spectrum shown in Fig. 2 is the sum of seven spectra, acquired with delays of

1 to 7 ms in 1-ms steps. The gate width was 1 ms, thus each spectrum shown is the integrated intensity from t =0.5 to 7.5 ms. Although it is well known that the trp excitation maximum is at 282 nm, and that trp does not have significant absorption at wavelengths longer than 300 nm, the phosphorescence intensity with 282-nm excitation was weaker than with 400-nm excitation. For the longer wavelength excitations (380 and 400-nm), the phosphorescence was blue shifted compared to shorter wavelength excitation (282 and 300 nm). For 380- and 400-nm excitation, trp exhibits two phosphorescence peaks at 480 and 525 nm. For excitation at 282 and 300 nm, only the phosphorescence peak at 525 nm was observed. Both the mechanism responsible for the shift in phosphorescence and the reason for the more intense phosphorescence at 400-nm excitation is not known. It may be due to dimers or trimers present in the trp powder.

Figures 3(a) and 3(b) show a 3-D representation of trp phosphorescence plotted as a function of wavelength and photodetector gate delay for λ_{ex}=300 and 400 nm, respectively. The emission intensity at 525 nm is plotted in Figs. 3(c) and 3(d) as a function of gate delay for λ_{ex}=300 and 400 nm, respectively. For λ_{ex}=300, the lifetime is 0.8 ms, and for λ_{ex}=400, the lifetime is 1.0 ms.

3.2 Phosphorescence from ex vivo Human Breast Tissues

Although the phosphorescence intensity in trp powder was greater for excitation at 400 nm than for excitation at 300 nm, tissues contain several fluorophores (NADH, collagen, and flavins) whose emission wavelengths can overlap with the trp phosphorescence. Therefore, the breast tissue
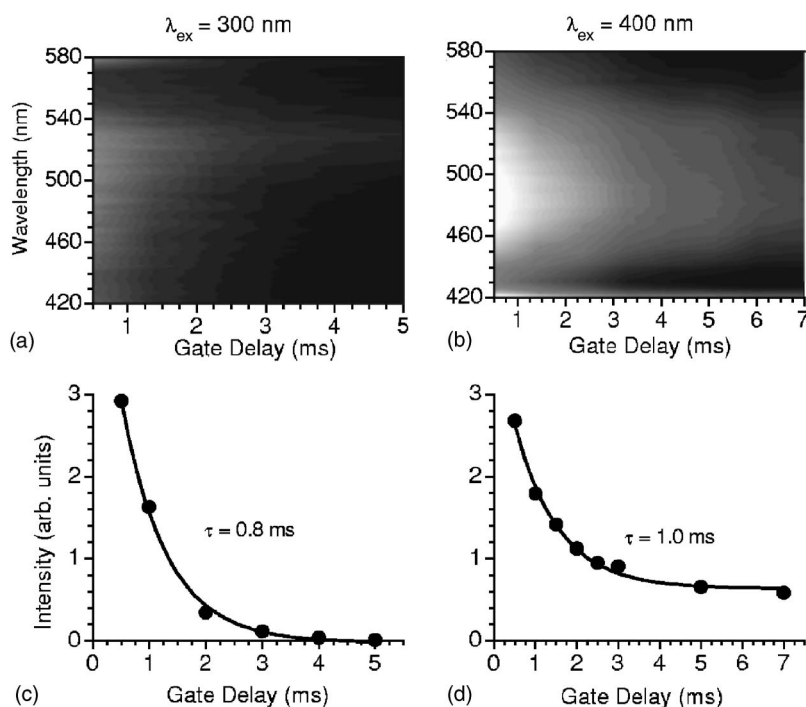

Fig. 3 Phosphorescence intensity of D-L tryptophan powder excited with (A) 300 and (B) 400 nm as a function of wavelength and gate delay. Intensity at 525 nm as a function of gate delay for (C) 300- and (D) 400-nm excitation.
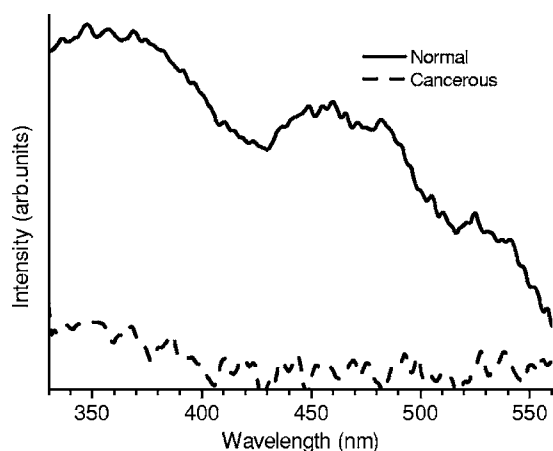
Fig. 4 Phosphorescence from normal and malignant glandular breast tissues. Signals were integrated for detector gate delays of 1 to 7 ms.

specimens were excited at 300 nm to reduce the contribution from these fluorophores.

The main types of tissue types found in human breast are glandular and adipose. Figure 4 shows the phosphorescence from *ex vivo* human normal and malignant breast tissues acquired with the CD-Scan. The plots shown in Fig. 4 are each the integration of seven spectra acquired with gate delays of 1 to 7 ms with 1-ms intervals. The normal tissues exhibited phosphorescence emission from 440 to 500 nm. Fluorescence can be also observed at 350 nm—most likely due to a long "tail" on the lamp emission. The normal tissues showed greater fluorescence and phosphorescence than the malignant tissues, which had almost no detectable phosphorescence.

Typical spectra, excited at 300 nm, from cancerous and normal glandular and adipose breast tissues are presented in Fig. 5. These spectra were acquired with the spectrograph system. The spectra have been normalized to unit maxima. The 2-s integration time enabled collection of both fluorescence and phosphorescence, and both types of emissions can be observed in Fig. 5. The CCD detector sensitivity is weaker
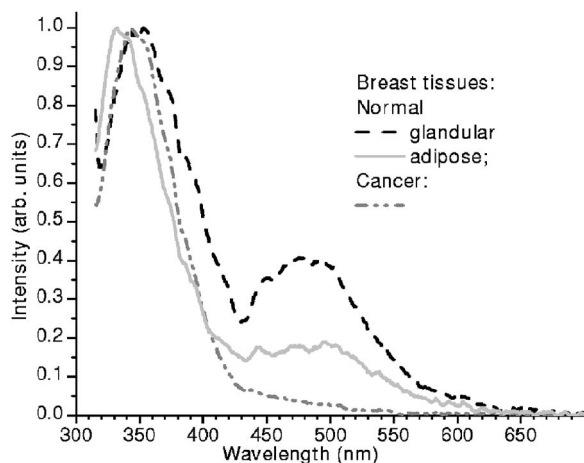

Fig. 6 Maps of (a) I_{345}/I_{500} ratio and (b) fluorescence peak position for normal gandular breast specimen.

in the UV than the visible, thus, the trp "counts" for fluorescence and phosphorescence do not differ as much as they would have if corrected for spectral response of the detector. Referring to Fig. 5, it can be observed that the adipose tissue with a fluorescence peak at 320 nm has a smaller Stokes shift than either the normal glandular or cancerous tissue. This may be a result of lower water content in adipose tissue. A broad trp phosphorescence band from 420 to 540 nm is observed in both the normal glandular and adipose tissues, which is not present in the cancerous tissues. The presence of trp phosphorescence in normal tissue but not in cancerous tissues suggests that the ratio of trp phosphorescence to fluorescence may be able to distinguish malignant breast tissue from normal glandular or adipose tissue. This difference can be quantified by computing the ratio of emission intensity at 345 nm (trp fluorescence) to the intensity at 500 nm (trp phosphorescence).

A map of the I_{345}/I_{500} ratio and positions of fluorescence peaks for a normal glandular specimen are shown in Figs. 6(a) and 6(b), respectively. Spectra were acquired at 50 locations on a ~4-$\times$4-mm specimen. The average value of the I_{345}/I_{500} ratio is 1.6±0.98 and the average fluorescence peak wavelength is 349±14 nm. Figures 7(a) and 7(b) plot the I_{345}/I_{500} ratio and fluorescence peak position for an adipose specimen, respectively. This specimen was also scanned at a

Fig. 5 Combined fluorescence and phosphorescence spectra of normal adipose and glandular breast and cancerous breast tissue. Excitation at 300 nm.
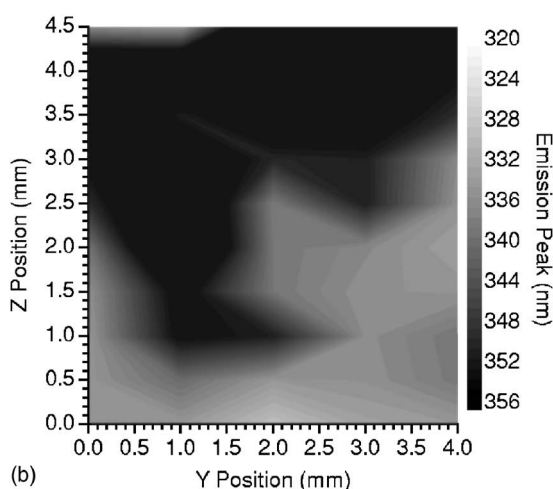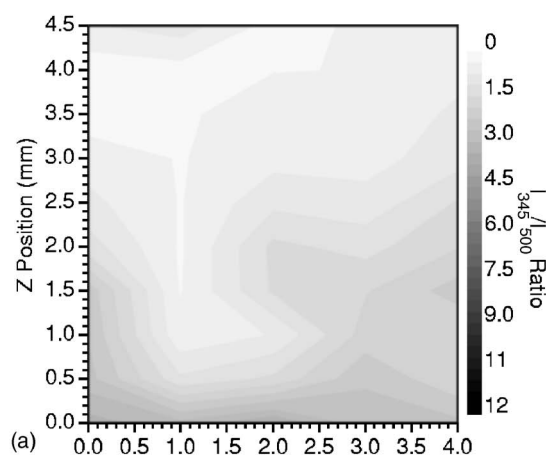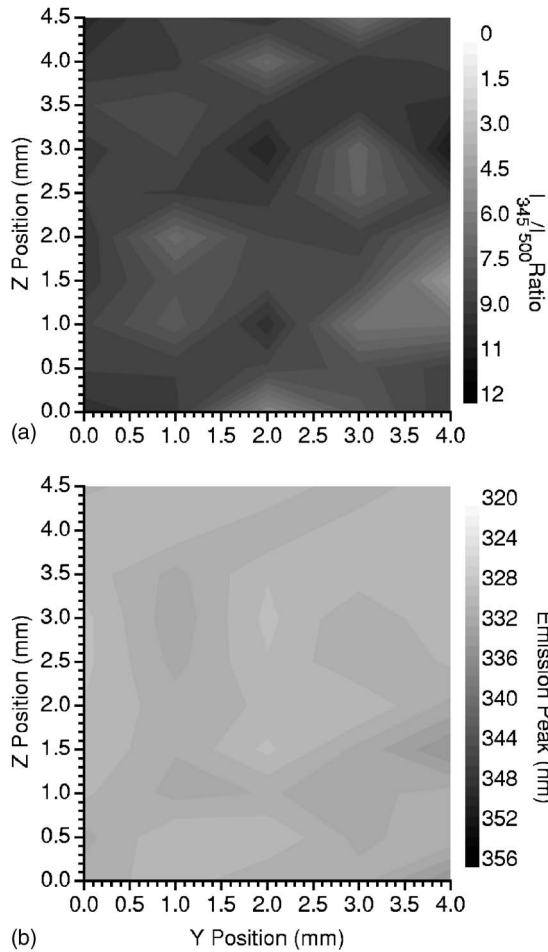
Fig. 7 Maps of (a) I_{345}/I_{500} ratio and (b) fluorescence peak position for adipose breast specimen.

Fig. 9 Maps of (a) I_{345}/I_{500} ratio from typical specimen and (b) location of fluorescence peak from same specimen. Right side of specimen is tumor, upper left is adipose tissue, and middle left is normal glandular.

total of 50 locations. The I_{345}/I_{500} ratio average value is 8.5 ± 1.14 and the fluorescence peak is at 331 ± 1 nm. The larger standard deviation in the Stokes shift of the glandular tissues reflects the greater variation in local protein environment in the glandular tissue, a result of its more complicated
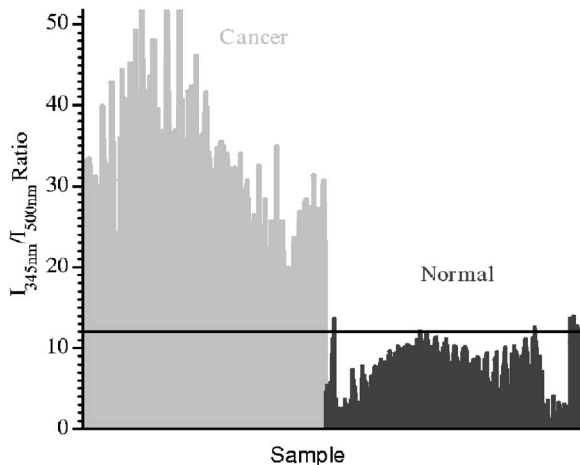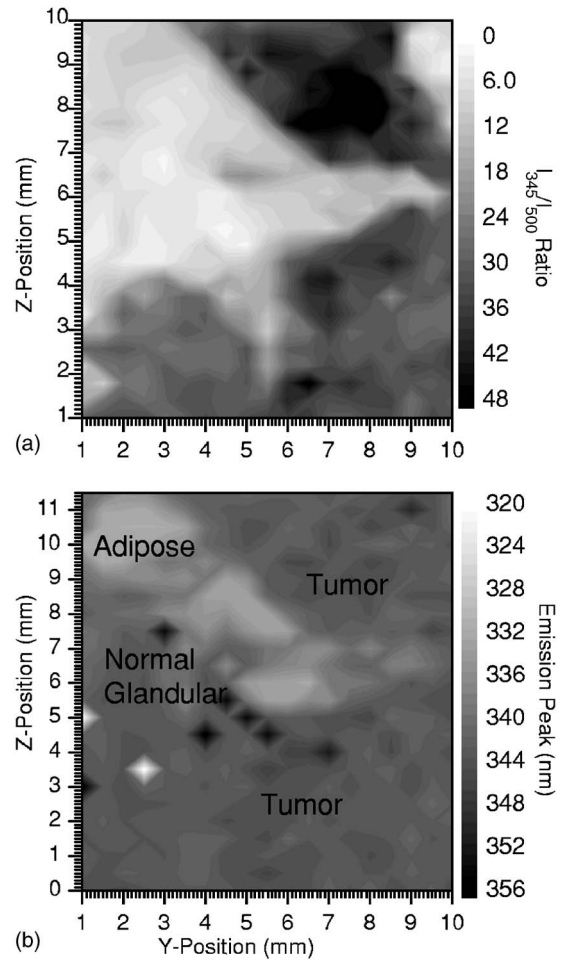

Fig. 8 Plot of I_{345}/I_{500} ratio for normal and cancerous breast tissues.

structure compared to fat tissue. The I_{345}/I_{500} ratio for the adipose specimen is a factor of 5 larger than for the glandular tissue, indicating the relatively weaker phosphorescence from fat. The Stokes shift for the adipose tissue is 18 nm less than for the glandular tissue, indicating that trp residue in fat tissues have less solvent (water) exposure than in glandular tissues.

The I_{345}/I_{500} ratio was calculated at 431 locations on malignant breast tissues and 455 locations on normal glandular and adipose tissues. These ratio values are plotted in Fig. 8. For the normal specimens (glandular and adipose) the I_{345}/I_{500} ratio is 6.6 ± 3.2 and for malignant specimens, the I_{345}/I_{500} ratio is 27.7 ± 12.6. Using a cutoff ratio value of 12, 421 of the 431 malignant and 446 of the 455 nonmalignant locations are correctly identified for a sensitivity of 97.6% and a specificity of 98%.

Figure 9(a) shows a map of the I_{345}/I_{500} ratio from a malignant breast tissue specimen. The specimen consists of a malignant tumor located on the right side of the figure, adipose tissue in the upper left, and regions of normal glandular tissue in the middle left. The malignant regions distinctly show a higher I_{345}/I_{500} ratio [darker regions in Fig. 9(a)] than

the adipose or normal glandular tissue. Figure 9(b) plots the location of the emission peak from the same specimen. The areas of adipose tissue had a smaller Stokes shift, i.e., shorter wavelength fluorescence [lighter regions in Fig. 9(b)] than glandular tissue.

4 Conclusions

This newly developed optical technique for cancer detection, based on phosphorescence and fluorescence spectroscopy, is fast, minimally invasive, and nondestructive. This technique may be applicable for either *in vivo* or *ex vivo* tissue analysis. The I_{345}/I_{500} ratio, with excitation at 300 nm, provides an excellent fingerprint for cancer detection in *ex vivo* tissues. The use of ratios, as markers for malignancy, enables comparison of data under different illumination conditions and with different surface structure. An I_{345}/I_{500} ratio of 0.5 to 5 corresponds to normal glandular breast tissue, a ratio of 5 to 12 corresponds the normal adipose breast tissue and a ratio higher than 12 indicates cancerous breast tissue. The Stokes shift information gives additional data for validation of the analysis. Since trp is present in practically every cell in the body, these fluorescence and phosphorescence fingerprints may be applicable in the detection of cancer at many different organ sites. Further research will be needed to confirm that the techniques applied here will provide accurate *in vivo* tissue diagnostic information.

This paper demonstrated that LEDs emitting in the UV can be used to excite native tissue fluorescence, which can advance the development of miniature instrumentation for optical biopsy.

References

1. R. Alfano, D. Tata, J. Cordero, P. Tomashefsky, F. Longo, and M. Alfano, "Laser induced fluorescence spectroscopy from native cancerous and normal tissue," *IEEE J. Quantum Electron.* **20**(12), 1507–1511 (1984).
2. R. Alfano, G. Tang, A. Pradhan, W. Lam, D. Choy, and E. Opher, "Fluorescence spectra from cancerous and normal human breast and lung tissues," *IEEE J. Quantum Electron.* **23**(10), 1806–1811 (1987).
3. R. R. Alfano, B. B. Das, J. Cleary, R. Prudente, and E. J. Celmer, "Light sheds light on cancer—distinguishing malignant tumors from benign tissues and tumors," *Bull. N. Y. Acad. Med.* **67**(2), 143–150 (1991).
4. B. B. Das, W. S. Glassman, R. R. Alfano, J. Cleary, R. Prudente, E. J. Celmer, and S. Lubicz, "UV-fluorescence spectroscopic technique in the diagnosis of breast, ovarian, uterus, and cervix cancer," in *Laser-Tissue Interaction II*, S. L. Jacques, Ed., *Proc. SPIE* **1427**, 368–373, (1991).
5. A. Katz, H. E. Savage, S. P. Schantz, S. A. McCormick, and R. R. Alfano, "Noninvasive native fluorescence imaging of head and neck tumors," *Technol. Cancer Res. Treat.* **1**(1), 9–15 (2002).
6. W. S. Glassman, C. H. Liu, G. C. Tang, S. Lubicz, and R. R. Alfano, "Ultraviolet excited fluorescence spectra from non-malignant and malignant tissues of the gynecological tract," *Lasers Life Sci.* **5**(1–2), 49–58 (1992).
7. Y. Yang, A. Katz, E. J. Celmer, M. Zurawska-Szczepaniak, and R. R. Alfano, "Optical spectroscopy of benign and malignant breast tissues," *Lasers Life Sci.* **7**(2), 115–127 (1996).
8. J. R. Lakowicz, *Principles of Fluorescence Spectroscopy*, Kluwer Academic, New York (1999).
9. G. Weber, "Fluorescence-polarization spectrum and electronic-energy transfer in tyrosine, tryptophan and related compounds," *Biochem. J.* **75**, 335–345 (1960).
10. B. Valeur and G. Weber, "Resolution of the fluorescence excitation spectrum of indole into the ^1L_a and ^1L_b excitation bands," *Photochem. Photobiol.* **25**, 441–444 (1977).
11. P. R. Callis, "^1L_a and ^1L_b transitions of tryptophan: applications of theory and experimental observations to fluorescence of proteins," *Methods Enzymol.* **278**, 113–150 (1997).
12. M. L. Saviotti and W. C. Galley, "Room temperature phosphorescence and the dynamic aspects of protein structure," *Proc. Natl. Acad. Sci. U.S.A.* **71**(10), 4154–4158 (1974).
13. Y. Kai and K. Imakubo, "Temperature dependence of the phosphorescence lifetimes of heterogeneous tryptophan residues in globular proteins between 293 and 77 K," *Photochem. Photobiol.* **29**, 261–265 (1979).
14. G. B. Strambini, P. Cioni, and R. A. Felicioli, "Characterization of tryptophan environments in glutamate dehydrogenases from temperature-dependent phosphorescence," *Biochemistry* **26**(16), 4968–4975 (1987).
15. J. M. Vanderkooi, D. B. Calhoun, and S. W. Englander, "On the prevalence of room-temperature protein phosphorescence," *Science* **236**(4801), 568–569 (1987).
16. D. B. Calhoun, S. W. Englander, W. W. Wright, and J. M. Vanderkooi, "Quenching of room temperature protein phosphorescence by added small molecules," *Biochemistry* **27**(22), 8466–8474 (1988).
17. G. B. Strambini and M. Gonnelli, "The indole nucleus triplet-state lifetime and its dependence on solvent microviscosity," *Chem. Phys. Lett.* **115**(2), 196–200 (1985).
18. V. Subramaniam, A. Gafni, and D. G. Steel, "Time-resolved tryptophan phosphorescence spectroscopy: a sensitive probe of protein folding and structure," *IEEE J. Sel. Top. Quantum Electron.* **2**(4), 1107–1114 (1996).
19. T. Truong, R. Bersohn, P. Brumer, C. K. Luk, and T. Tao, "Effect of pH on the phosphorescence of tryptophan, tyrosine, and proteins," *J. Biol. Chem.* **242**(12), 2979–2985 (1967).
20. E. G. Strambini and G. B. Strambini, "Tryptophan phosphorescence as a monitor of protein conformation in molecular films," *Biosens. Bioelectron.* **15**(9–10), 483–490 (2000).
21. J. A. Schauerte, D. G. Steel, and A. Gafni, "Time-resolved room temperature tryptophan phosphorescence in proteins," *Methods Enzymol.* **278**, 49–71 (1997).
22. A. K. Brewer, "The high pH therapy for cancer tests on mice and humans," *Pharmacol., Biochem. Behav.* **21**(Suppl. 1), 1–5 (1984).
23. A. Alimova, A. Katz, V. Sriramoju, Y. Budansky, A. A. Bykov, R. Zeylikovich and R. R. Alfano, "Hybrid native phosphorescence and fluorescence spectroscopy for cancer detection," in *Optical Biopsy VI*, A. Katz and R. R. Alfano, Eds., *Proc. SPIE* **6091**, 22–25 (2006).
24. L. Wang, G. Zhang, J. C. Luo, F. Zeng, Q. Z. Wang, S. A. Alfano, A. Katz, M. Zevallos, and R. R. Alfano, "Wireless spectroscopic compact photonic explorer for diagnostic optical imaging," *Biomed. Microdevices* **7**(2), 111–115 (2005).